Small-molecule agonists of mammalian Diaphanous–related (mDia) formins reveal an effective glioblastoma anti-invasion strategy

Jessica D. Arden[a], Kari I. Lavik[a], Kaitlin A. Rubinic[a], Nicolas Chiaia[b], Sadik A. Khuder[c], Marthe J. Howard[b], Andrea L. Nestor-Kalinoski[d], Arthur S. Alberts[e], and Kathryn M. Eisenmann[a]

[a]Department of Biochemistry and Cancer Biology, [b]Department of Neurosciences, [c]Departments of Medicine and Public Health and Homeland Security, and [d]Department of Surgery, University of Toledo Health Science Campus, Toledo, OH 43614; [e]Laboratory of Cell Structure and Signal Integration, Van Andel Research Institute, Grand Rapids, MI 49503

ABSTRACT **The extensive invasive capacity of glioblastoma (GBM) makes it resistant to surgery, radiotherapy, and chemotherapy and thus makes it lethal. In vivo, GBM invasion is mediated by Rho GTPases through unidentified downstream effectors. Mammalian Diaphanous (mDia) family formins are Rho-directed effectors that regulate the F-actin cytoskeleton to support tumor cell motility. Historically, anti-invasion strategies focused upon mDia inhibition, whereas activation remained unexplored. The recent development of small molecules directly inhibiting or activating mDia-driven F-actin assembly that supports motility allows for exploration of their role in GBM. We used the formin inhibitor SMIFH2 and mDia agonists IMM-01/-02 and mDia2-DAD peptides, which disrupt autoinhibition, to examine the roles of mDia inactivation versus activation in GBM cell migration and invasion in vitro and in an ex vivo brain slice invasion model. Inhibiting mDia suppressed directional migration and spheroid invasion while preserving intrinsic random migration. mDia agonism abrogated both random intrinsic and directional migration and halted U87 spheroid invasion in ex vivo brain slices. Thus mDia agonism is a superior GBM anti-invasion strategy. We conclude that formin agonism impedes the most dangerous GBM component—tumor spread into surrounding healthy tissue. Formin activation impairs novel aspects of transformed cells and informs the development of anti-GBM invasion strategies.**

Monitoring Editor
Carole Parent
National Institutes of Health

Received: Nov 4, 2014
Revised: Aug 31, 2015
Accepted: Sep 4, 2015

INTRODUCTION

Glioblastoma (GBM) is the most frequently diagnosed primary malignant brain tumor in adults (Dolecek *et al.*, 2012). Standard therapy of surgical resection followed by temozolomide and radiation extends survival by only months (Grossman *et al.*, 2010). Individual cells migrate up to several centimeters from the primary tumor (Giese *et al.*, 1996) and compromise essential CNS function (Batchelor *et al.*, 2013). Because tumors lack an easily defined margin, complete surgical resection is impossible and precise radiotherapy is difficult (Berens and Giese, 1999). Refractory cells escape, invade, and give rise to recurrent disease (Giese *et al.*, 2003; Lefranc *et al.*, 2005). In addition, invasive GBM cells are more resistant to radiotherapy (Milano *et al.*, 2010) and chemotherapy (Nakada *et al.*, 2007) than noninvasive counterparts. An inverse correlation between cell motility and proliferation exists, in that genes driving proliferation are down-regulated in migrating GBM cells (Mariani *et al.*, 2001). Therefore inhibiting invasion would not only limit the spread of disease, but it also might sensitize cells to conventional therapies (Berens and Giese, 1999).

Tumor cell invasion relies upon coordinated assembly and disassembly of the actin cytoskeleton that physically supports cell structures. Mammalian Diaphanous (mDia)–related formins (mDia1, 2, and 3) are effectors for Rho GTP-binding proteins in establishing and

This article was published online ahead of print in MBoC in Press (http://www.molbiolcell.org/cgi/doi/10.1091/mbc.E14-11-1502) on September 9, 2015.

Address correspondence to: Kathryn M. Eisenmann (Kathryn.eisenmann@utoledo.edu).

Abbreviations used: DAD, Diaphanous autoregulatory domain; GBM, glioblastoma; IMM, intramimic; mDia formin, mammalian diaphanous–related formin.

maintaining polarized cell adhesion, migration, and division in both normal and malignant cells (Chesarone *et al.*, 2010). The gene/protein nomenclature is complicated; human mDia proteins are also referred to as Dia, DIAPH, hDia, or Drf and are encoded by the *DIAPH/DRF* genes. For example, human mDia2 protein is encoded by the *DIAPH3*/*DRF3* gene, whereas mDia1 protein is encoded by *DIAPH1/DRF1*. For simplicity, we will refer to the original mDia1 and mDia2 genes and proteins under study here (Watanabe *et al.*, 1997; Alberts *et al.*, 1998a). GTP-bound Rho proteins bind to and allosterically disrupt an autoinhibition mechanism between the Dia-inhibitory and Dia-autoregulatory domains (DID and DAD, respectively) that flank the formin homology-1 and -2 (FH1 and FH2) domains (Lammers *et al.*, 2005; Nezami *et al.*, 2006). The FH2 domain generates linear actin filaments through a processive elongation mechanism (Wallar and Alberts, 2003; Harris *et al.*, 2006; Kovar, 2006; Baarlink *et al.*, 2010; DeWard *et al.*, 2010). Although several small molecules inhibiting mDia formins exist, solubility issues limit the use of most reagents in cell culture. Only the small-molecule inhibitor SMIFH2 affects mDia-mediated functions in living cells, including cell motility (Gauvin *et al.*, 2009). Conversely, the small molecules intramimic-01 (IMM-01) and IMM-02 activate mDia2 by disrupting the autoinhibitory DID-DAD interaction and function as mDia agonists (Lash *et al.*, 2013). IMM-01 and -02 induce F-actin assembly and stabilize microtubules in cells and as a consequence cause cell-cycle arrest, apoptosis and impair tumorigenesis from xenografted tumor cells implanted into immune-deficient mice (Lash *et al.*, 2013).

Owing to their critical roles in regulating tumor cell migration and invasion, we evaluated mDia inhibition and activation to determine whether either strategy has potential as a clinical intervention in GBM treatment. We showed that either functional inhibition or suppression of mDia expression negatively affected persistent migration in two dimensions, yet the cells remained motile. Conversely, activation through dominant-active mDia2 expression or IMM-01/02 incubation dramatically suppressed both net migration and total distance migrated. In both Transwell and spheroid invasion assays, mDia activation was superior to inactivation in blocking invasion. Finally, IMM-mediated mDia2 agonism blocked GBM spheroid cellular invasion in a rat brain slice invasion model. These findings indicate that agonism may represent an effective and clinically relevant GBM therapeutic strategy.

RESULTS

mDia expression in GBM clinical samples and invasive cell lines

To explore a possible role for mDia formins in GBM, we examined their expression in clinical samples. Expression of *DIAPH1* and *DIAPH3* (encoding mDia1 and mDia2, respectively) was assessed in noncancerous human brain and grades I–IV glioma by analyzing previously published Affymetrix whole-genome expression array data using probes corresponding to the mDia1 and mDia2 FH2 domains (Gravendeel *et al.*, 2009). DIAPH1 expression in high-grade glioma was equivalent to nonglioma controls, although it was slightly elevated in grade II and reduced in grade I glioma (Figure 1A). In contrast, *DIAPH3* expression was elevated in grades II, III, and IV glioma relative to normal brain and to grade I glioma (Figure 1B).

Next we examined a panel of human GBM cell lines for mDia protein expression. All cell lines expressed mDia1 and mDia2, although levels varied (Figure 1C). Our remaining studies were conducted with invasive U251 or U87 cell lines (Strojnik *et al.*, 2006; Radaelli *et al.*, 2009; Hsieh *et al.*, 2012). We evaluated the spatial localization of endogenous mDia proteins, and in both cell lines mDia1 was diffusely cytoplasmic, with some colocalization in F-actin–enriched areas on the cell periphery (Figure 1, D and E). mDia2 exhibited nuclear and cytoplasmic localization. This is consistent with previous reports in a host of tumor and nontumor cell types (Peng *et al.*, 2003; Eisenmann *et al.*, 2007b; Gupton *et al.*, 2007; Watanabe *et al.*, 2008; Gorelik *et al.*, 2011; Pettee *et al.*, 2014).

Requirement for mDia in U251 persistent migration

To evaluate mDia's role in GBM migration in two dimensions, we performed scratch assays (Figure 2A) and tracked individual cell migratory paths for 24 h postscratch (Supplemental Figure S1). We calculated the total distance cells moved (*T*), the net distance or the portion of total distance migrated that moves a cell toward the scratch center (*D*), cell velocity (*T*/time in hours), and the persistence (*D*/*T*) (Figure 2, B–G).

We tracked the migration paths of U251 cells expressing dominant-negative yellow fluorescent protein (YFP)–mDia1-FH2ΔN, which interferes with both mDia1- and mDia2-driven F-actin assembly (Copeland and Treisman, 2002; Eisenmann *et al.*, 2007b; Figure 2D confirms plasmid expression). Cells were also treated with SMIFH2, a small-molecule mDia formin inhibitor (Rizvi *et al.*, 2009), or were transfected with mDia1 or mDia2 small interfering RNA (siRNA; Supplemental Figure S2).

To initially assess functional inhibition of mDia in SMIFH2-treated U251 cells, we used an SRE-lacZ reporter assay (Figure 2H; Alberts *et al.*, 1998b). Of interest, serum response factor (SRF) activation was unaffected by SMIFH2 treatment in the presence of serum. The inability of formin inhibition by SMIFH2 to effectively block SRF activation is not altogether surprising. SRF senses changes in actin monomer content created by changes in assembly and disassembly by multiple mechanisms. For example, LIM-kinase, which stabilizes F-actin by inactivating F-actin severing by cofilin, is a potent activator of SRF. Similarly, vasodilatator-stimulated phosphoprotein and Wiskott–Aldrich syndrome protein–activated Arp2/3 alteration of G-actin pools activates SRF (Sotiropoulos *et al.*, 1999; Geneste *et al.*, 2002; Grosse *et al.*, 2003). Each of these activities constitutes essential processes needed to create cell structure components by SRF (α, β, γ-actin) during cellular replication and regeneration, and so biology has created multiple avenues in addition to formins to affect new gene expression in the nucleus. However, functional readouts of cellular F-actin content and microtubule stability revealed that SMIFH2 treatment was affecting both F-actin and microtubule dynamics (Supplemental Figures S3–S5, respectively). To assess whether changes in microtubule dynamics were equally influenced by SMIFH2, we treated U251 monolayers with SMIFH2 and assessed global levels of β-tubulin as well as microtubule stabilization through Western blotting for detyrosinated tubulin (Supplemental Figure S5). Short-term (1–2 h) SMIFH2 treatment negatively affected both β-tubulin levels and detyrosination, suggesting that the mechanism of action for SMIFH2 could be twofold, affecting both microtubule and F-actin dynamics. Longer-term incubation of cells with SMIFH2 did not reveal similar effects, perhaps due to drug stability, as previously postulated (Isogai *et al.*, 2015).

Loss of mDia expression/activity did not dramatically affect the total distance migrated by U251 cells over 24 h (Figure 2C). The total distance migrated was modestly reduced in cells expressing YFP-mDia1-FH2ΔN (by 12%) or mDia2 siRNA (17%) and in SMIFH2-treated cells (15%). In contrast, net distance was significantly and dramatically reduced by 62, 50, and 59%, respectively (Figure 2E). Of interest, cell velocities were unaffected by mDia suppression (Figure 2F). Finally, mDia depletion or functional inhibition revealed significantly reduced persistence, likely attributed to wandering paths of still relatively motile individual cells (Figure 2F and Supplemental Figure S1).

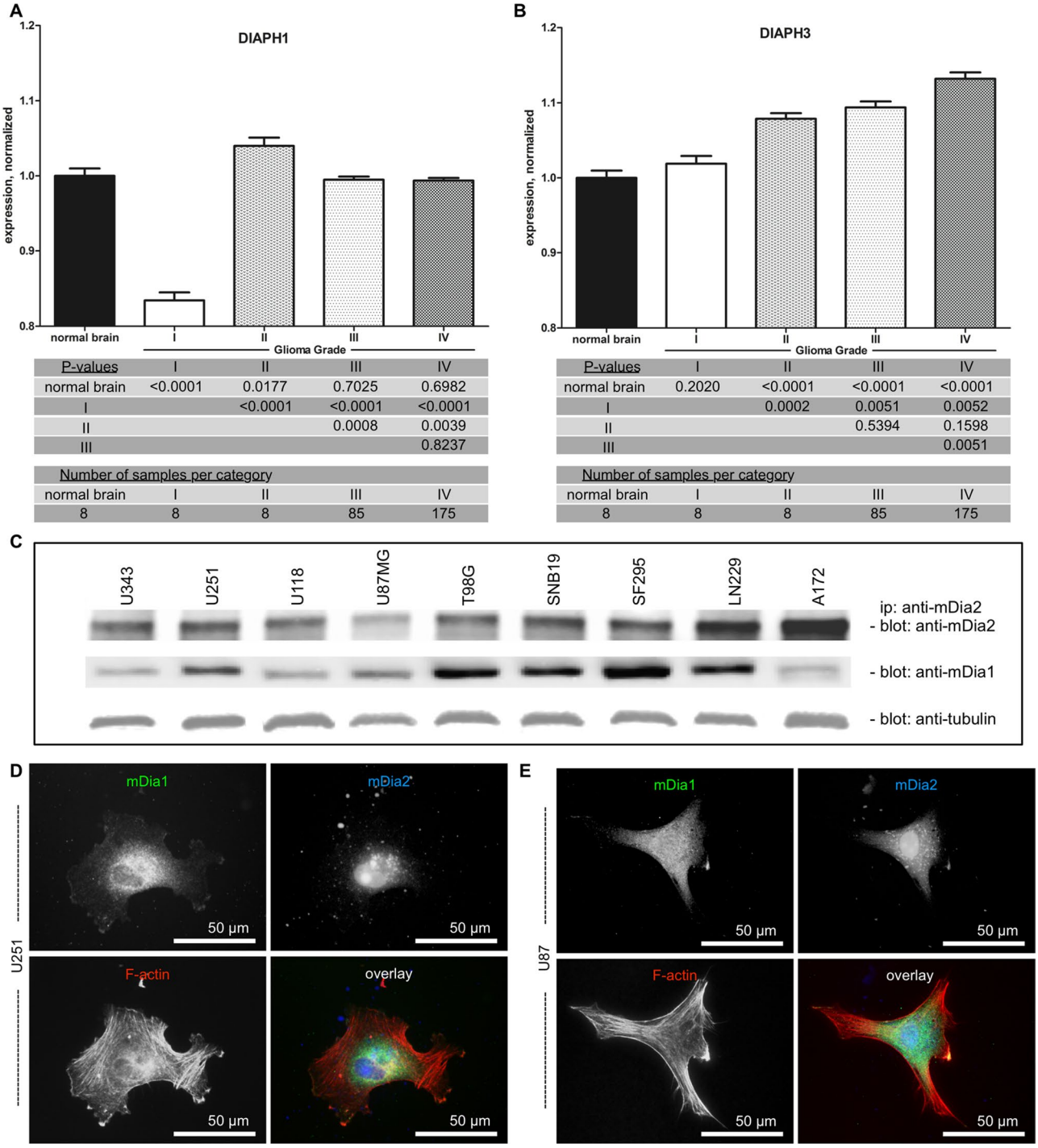

P-values	I	II	III	IV
normal brain	<0.0001	0.0177	0.7025	0.6982
I		<0.0001	<0.0001	<0.0001
II			0.0008	0.0039
III				0.8237

Number of samples per category				
normal brain	I	II	III	IV
8	8	8	85	175

P-values	I	II	III	IV
normal brain	0.2020	<0.0001	<0.0001	<0.0001
I		0.0002	0.0051	0.0052
II			0.5394	0.1598
III				0.0051

Number of samples per category				
normal brain	I	II	III	IV
8	8	8	85	175

FIGURE 1: mDia formin expression in human glioma and glioblastoma cell lines. (A, B) Expression of *DIAPH1*, encoding mDia1 (A), and *DIAPH3*, encoding mDia2 (B), in normal human brain and glioma samples as assessed by Affymetrix whole-genome expression array (Gravendeel *et al.*, 2009). *p* values are indicated below the graphs. Error bars indicate SD. (C) mDia1 and mDia2 protein expression in a panel of human glioblastoma cell lines as assessed by Western blot and immunoprecipitation, respectively. (D, E), mDia1 and mDia2 expression and localization in U251 (D) and U87 (E) cells as assessed by immunofluorescence.

mDia activation blocks U251 cell motility

We next examined the effects of constitutive mDia activation on U251 directionality and the total distance migrated. mDia activation can act to stabilize both the F-actin and microtubule cytoskeletons (Alberts, 2001; Palazzo *et al.*, 2001; Lash *et al.*, 2013), preventing turnover of motility structures necessary for migration. We tracked the migration of cells expressing YFP-mDia2-ΔGBD (Tominaga *et al.*, 2000) and cells treated with the agonist IMM-01 or IMM-02 (Supplemental Figure S1). IMM drugs were previously shown to agonize mDia2 and play a role in both F-actin dynamics (by blocking mDia DID-DAD binding) and microtubule stabilization in NIH 3T3 and, to a lesser extent, SW480 cells (Lash *et al.*, 2013). As

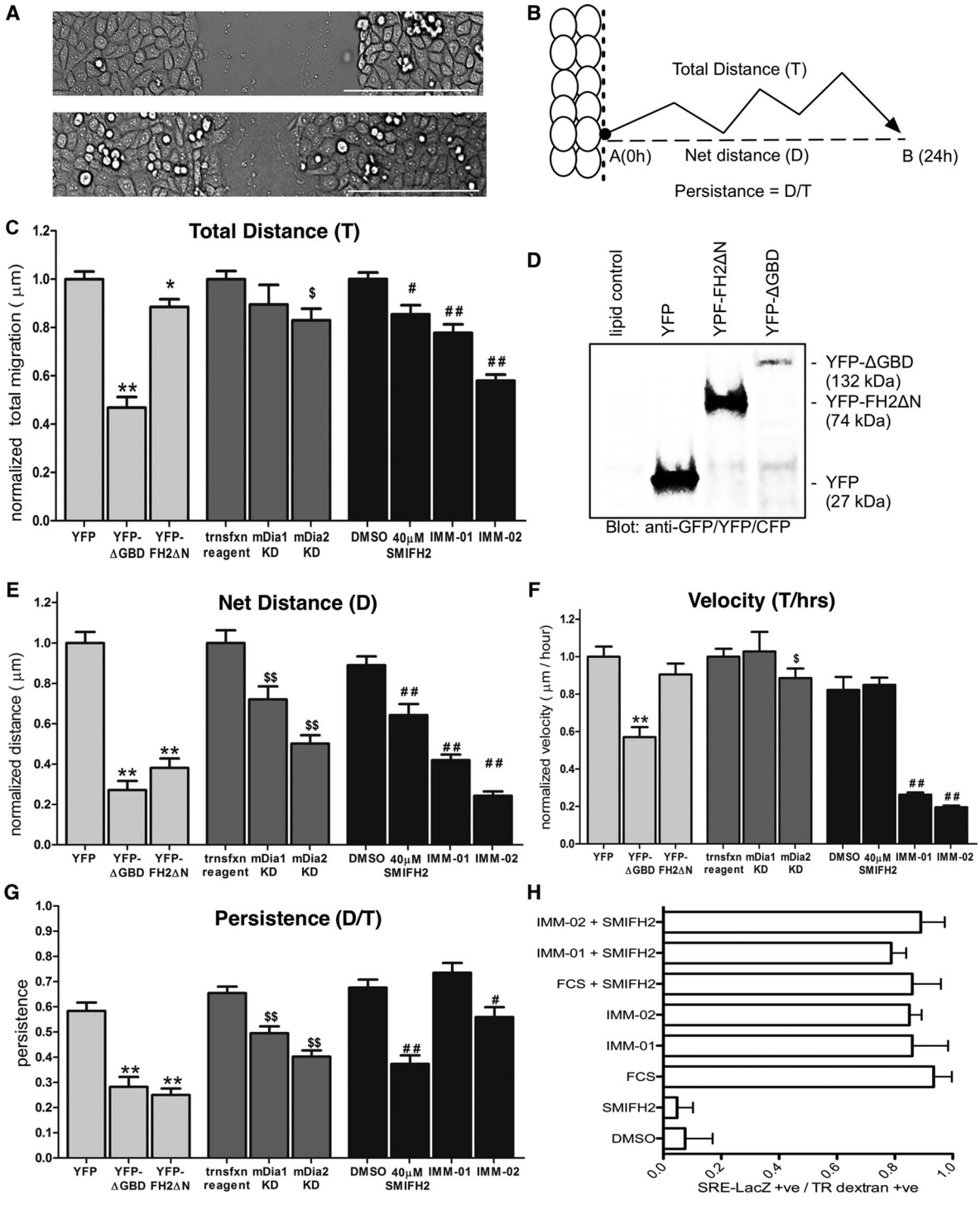

FIGURE 2: mDia formins are required for persistent U251 glioblastoma cell migration. (A) Wound-healing assays using U251 cells plated to confluence. Scratches were introduced and imaged every 30 min for 24 h. Representative 10× images. (B) U251 cells were transfected with YFP, dominant-negative YFP-mDia YFP-FH2ΔN, or constitutively active YFP-ΔGBD; or cells were treated with 40 μM SMIFH2; or transfected with siRNA against mDia1 or mDia2. Persistent migration was calculated by measuring the net distance, *D*, between the cell start (point A) and finish (point B) and dividing by the total distance migrated, *T*. (C) A minimum of 20 cells per condition was tracked. *p* values are relative to YFP (*), transfection reagent controls ($), or DMSO (#). $^{*,\$,\#}p < 0.05$; $^{**,\$\$,\#\#}p < 0.0001$. Error bars indicate SD. (D) U251 cells were transfected with lipid or with YFP, YFP-FH2ΔN, or YFP-ΔGBD, and lysates were collected after 24 h. Overexpression was assessed by Western blotting. (E–G) Values of *D*, velocity (*T*/time in hours), and persistence (*D*/*T*) were calculated for a minimum of 20 cells tracked per condition. Each experiment was performed at least thrice. (H) U251 cells were microinjected with reporter plasmid encoding SRE-LacZ, and Texas red as a marker for microinjection. After 1 h, cells were treated for 4 h with 10% (vol/vol) FBS, DMSO, 40 μM SMIFH2, or 100 μM IMM-01 or IMM-02, alone or in combination as indicated. Bars represent mean ± SD from three experiments in which 20–40 cells were microinjected for each condition.

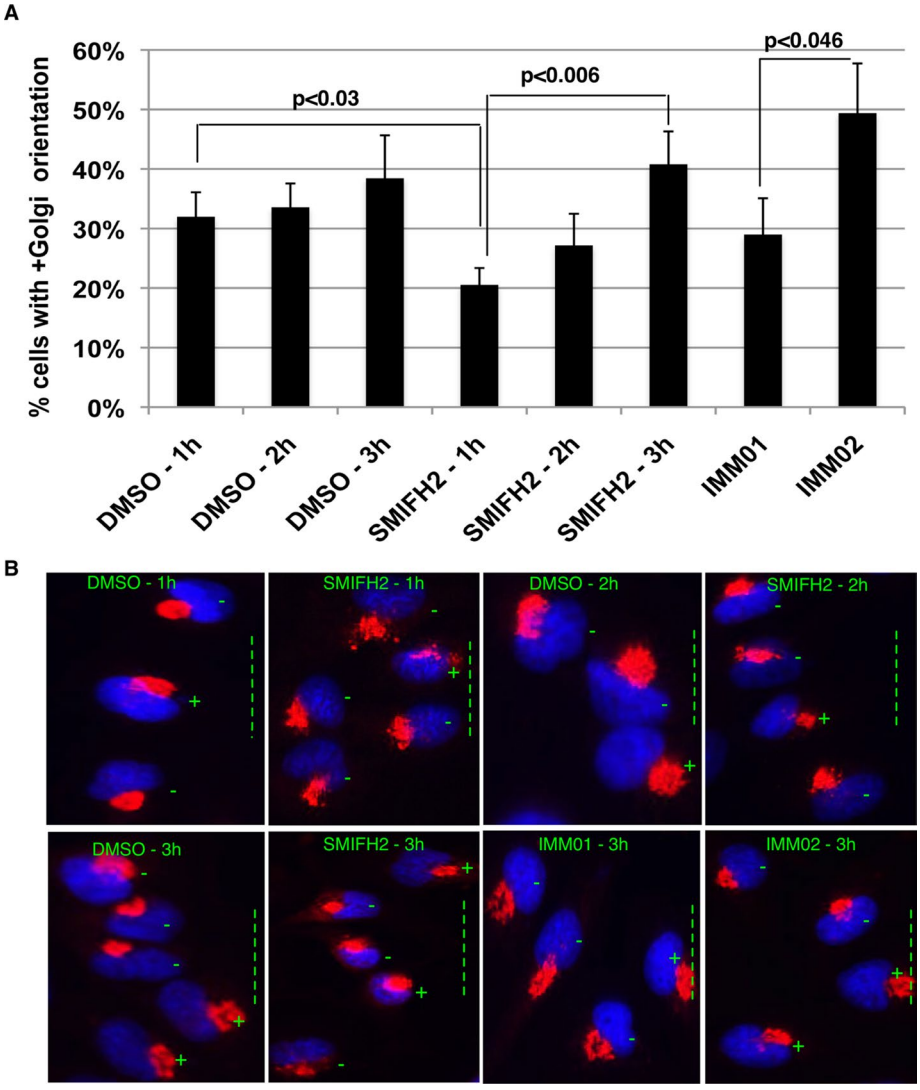

FIGURE 3: Altered mDia functional activity affects Golgi polarity and morphology in migrating U251 cells. (A) Confluent U251 cells were scratched and simultaneously treated with DMSO, 100 μM IMM-01, 100 μM IMM-02, or 40 μM SMIFH2 and were allowed to migrate for 1–3 h. Cells were stained with gm130 antibodies (red) to visualize the Golgi and DAPI (blue). At least 30 cells from at least two independent experiments were imaged for >60 cells counted per condition. Quadrants were drawn on cells, with the plus quadrant facing the wound. Positive (+) cells had gm130 staining falling in the front quadrant. Negative cells (–) had gm130 staining falling in one or more of the adjacent quadrants. Values are represented as averages ± SD. (B) Representative 40× images.

shown in Figure 2H, IMM drugs induced SRF activity in a reporter system in U251 cells, indicating enhanced actin dynamics. Increases in cellular F-actin content were also observed in the time frames tested (Supplemental Figures S3 and S4). Of interest, we failed to see increases in either β-tubulin levels or detyrosination in response to IMM through 2 h, whereas incubation with Taxol dramatically enhanced microtubule stabilization. These data indicated that in U251 cells, IMMs were primarily affecting F-actin dynamics. Functional activation of mDia proteins significantly inhibited both total distance and net distance and dramatically reduced cell velocities (Figure 2, C, E, and F). YFP-mDia2-ΔGBD expression and IMM-02 treatment were the most potent inhibitors of persistent migration; IMM-01 treatment effects were less dramatic, but this was attributed to the relatively equal inhibition of both variables used in the persistent migration calculation.

Altered mDia functional activity affects Golgi polarity in migrating U251 cells

Changes in formin functional activity were previously linked to defects in Golgi polarity (Zaoui *et al.*, 2008; Ang *et al.*, 2010; Colon-Franco *et al.*, 2011; Zilberman *et al.*, 2011; Isogai *et al.*, 2015) in U2OS, HCT116, and other cell lines. We therefore assessed whether the Golgi failed to align in the direction of U251 migration in a scratch assay. During cell migration, the Golgi typically aligns in front of the nucleus in the direction of migration. We visualized the Golgi in migrating cells by staining with anti-gm130 Golgi marker antibodies and quantified Golgi polarity in the direction of a wound. Indeed, whereas the Golgi was visualized as a large punctate structure aligned in the front of the nucleus in the direction of the wound in 30–40% of untreated or dimethyl sulfoxide (DMSO)–treated cells (Figure 3, A and B; dashed green line indicates wound), cells treated with SMIFH2 for 1 h had a significant reduction in the percentage of cells with a polarized Golgi. This was overcome over longer treatments (through 3 h), potentially due to drug stability (Isogai *et al.*, 2015). These results indicate a role for mDia-mediated F-actin dynamics in establishing Golgi polarity, which is critical for cell migration, and these findings agree with previous reports in U2OS and HCT116 cells using mDia dominant-negative expression or SMIFH2 treatment (Zilberman *et al.*, 2011; Isogai *et al.*, 2015). Of interest, there was no increase in Golgi polarity in IMM-01–treated cells relative to controls. Although there was a ~25% increase in Golgi polarity due to IMM-02 treatment relative to DMSO controls, this was not statistically significant.

Altered mDia activity reduces chemotactic single-cell invasion

We next sought to determine whether mDia activation or suppression affected invasion through Matrigel. U87 (Figure 4, A–C) cells were treated with SMIFH2, IMM-01, or IMM-02, and Transwell invasion assays were performed. Whereas DMSO-treated cells invaded toward fetal bovine serum (FBS) relative to serum-free controls, both mDia inhibition and activation significantly inhibited invasion (Figure 3, A–C). Similar results were achieved in U251 cells (Supplemental Figure S6).

mDia inhibition and/or depletion reduces spheroid invasion

Whereas both inhibition and activation impaired single-cell chemotaxis through Transwells, these assays are an incomplete representation of GBM invasion compared with a primary tumor. Therefore we assessed invasion using a spheroid invasion assay, which measures the invasive capacity of a multicellular mass in three-dimensional (3D) space, which is more representative of in vivo conditions (Del Duca *et al.*, 2004). U87 and U251 spheroids were formed, embedded in Matrigel, and invaded for 48 h. Spheroid invasion was

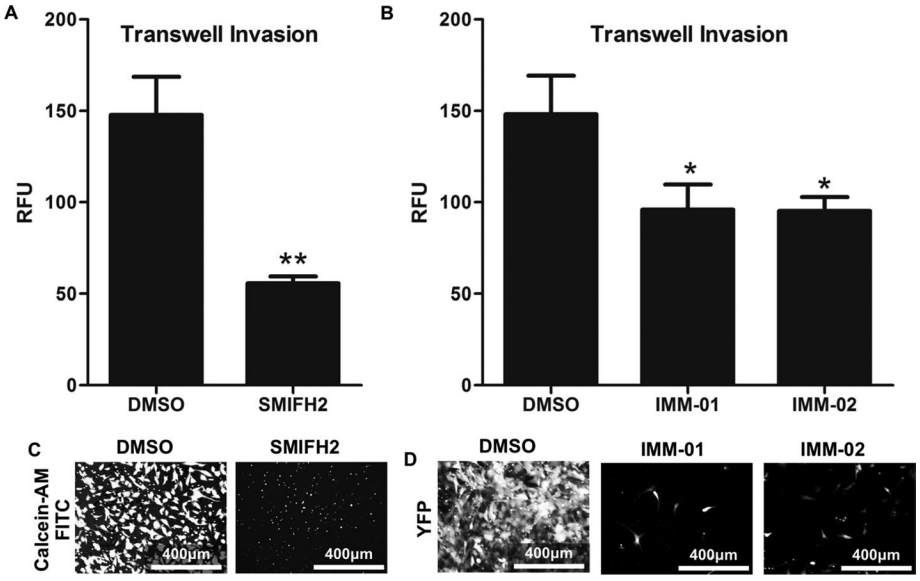

FIGURE 4: Both mDia inhibition and agonism inhibit GBM Transwell invasion. (A, B), U87 cells treated with 40 μM SMIFH2 or 100 μM IMM-01 or IMM-02 invaded for 48 h through Transwells coated with GFR Matrigel. Values are expressed as RFUs. *p* values are relative to DMSO. **p* <0.05; ***p* < 0.001. Error bars indicate SD. (C) Representative 10× images after 48-h invasion.

measured by drawing a region of interest around the perimeter of the invasive front. Spheroids were measured upon embedding (*T*0) (Supplemental Figure S7) and after 24 and 48 h. SMIFH2 treatment significantly inhibited U87 (Figure 5) and U251 (Supplemental Figure S8) spheroid invasion relative to controls, although SMIFH2-treated spheroids were still invasive. Cells on the periphery of SMIFH2-treated spheroids exhibited an invasive phenotype similar to control spheroids (Supplemental Movies S1 and S2). Thus loss of mDia activity slowed spheroid invasion but was not sufficient to completely inhibit it.

To determine whether the effects of SMIFH2 were mediated through inhibition of mDia1, mDia2, or both, we assessed U87 spheroid invasion after mDia1 and mDia2 depletion (Supplemental Figure S2). After siRNA treatment of monolayers for 48 h, spheroids were formed for 72 h. Spheroids were embedded in Matrigel and invaded for 48 h; this corresponded to 120–168 h after siRNA treatment, when mDia expression was completely suppressed (Supplemental Figure S2, C and D, and Figure 6A). Both mDia1 and mDia2 depletion significantly impaired spheroid invasion at both 24 and 48 h after embedding (Figure 6, B and C), comparable to SMIFH2 treatment. This confirms that mDia loss slows but does not block invasion.

mDia activation inhibits spheroid invasion

We next determined whether mDia activation is more effective than mDia inhibition at suppressing spheroid invasion. U87 spheroids were pretreated with 100 μM IMM-01 or IMM-02 or DMSO for 24 h before embedding. Spheroids invaded for 48 h either in the absence of drug ("pre-trx") or with continuous 100 μM IMM-01 or IMM-02 ("contin.") treatment. IMM-01 pretreatment significantly reduced invasion at 24 but not 48 h; this is likely because the IMM-01 pharmacodynamic profile requires frequent dosing to maintain continuous mDia agonism (Figure 7A). In contrast, IMM-02 pretreatment significantly reduced invasion (Figure 7A). However, continuous IMM-01 or IMM-02 treatment was most effective at blocking spheroid invasion (Figure 7A).

Unlike control and SMIFH2-treated spheroids, on whose edges protrusive cells invade away from the core, spheroids treated with IMM-01 or IMM-02 have smooth, noninvasive edges (Figure 7, B and C, and Supplemental Movie S3). Washout experiments and DRAQ7 viability staining (Figures 7C and Supplemental Figure S9) confirmed that this lack of invasion was not the consequence of reduced cell viability but was the result of diminished invasive capacity. Whereas IMM-01 and -02 continuous treatments blocked invasion through 48 h, upon removal of either compound, spheroid invasion resumed (Supplemental Figure S9). This was confirmed in flow-cytometric cell cycle analysis: monolayers treated for 24–120 h

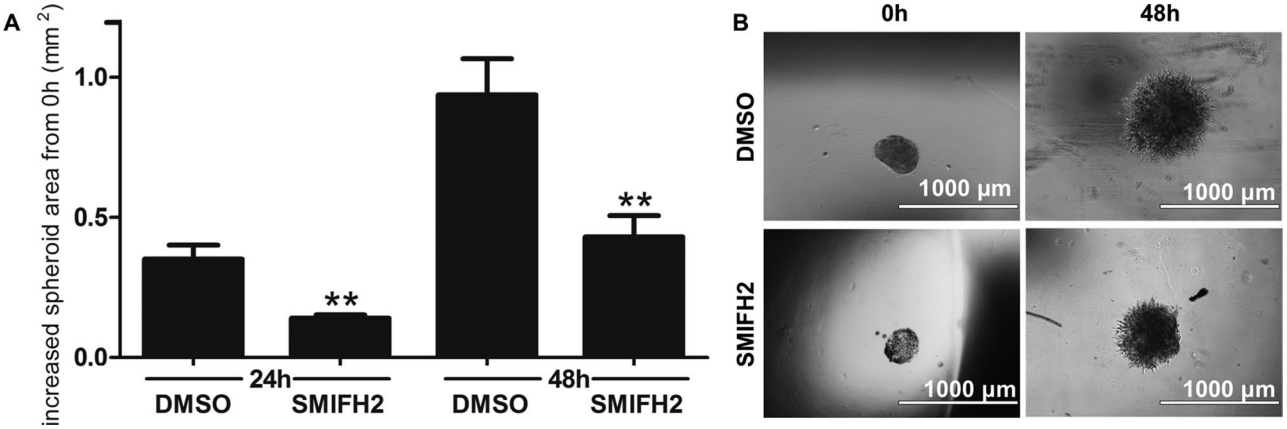

FIGURE 5: mDia inhibition diminishes GBM spheroid invasion. (A) U87 spheroids were formed for 72 h and embedded in GFR Matrigel. Spheroids were treated with DMSO or 40 μM SMIFH2. To quantify invasion, spheroids were imaged 0, 24, and 48 h after embedding, and the change in surface area was measured. *p* values are relative to DMSO control. ***p* < 0.001. All data are expressed as average ± SD. (B) Representative 4× bright-field images after 48-h invasion.

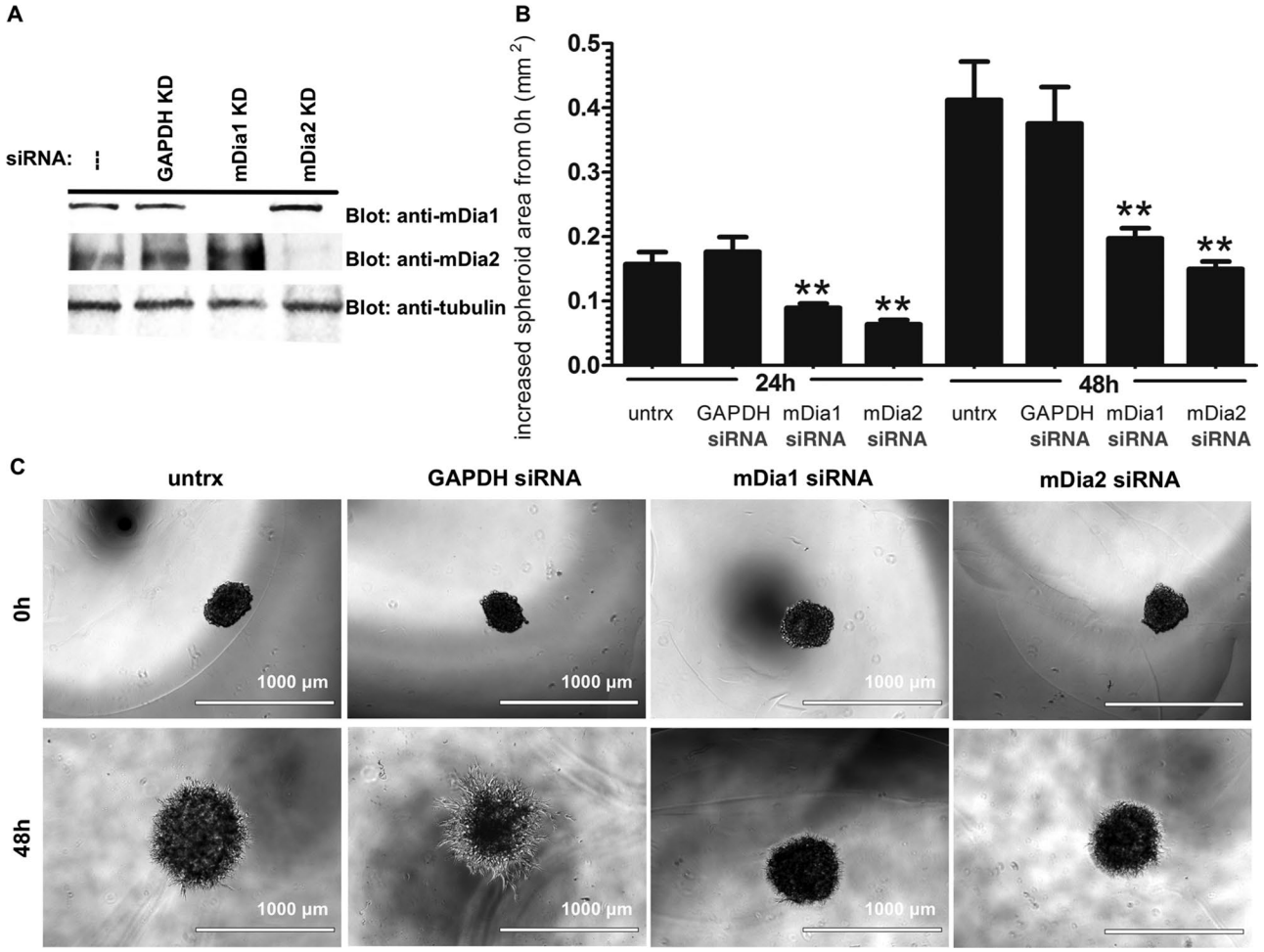

FIGURE 6: mDia1 and mDia2 depletion reduces spheroid invasion. (A) Western blotting of lysates collected 144 h after siRNA treatment (corresponding to 24 h after spheroid embedding) confirmed mDia1 and mDia2 depletion. (B) YFP-U87 spheroids were formed 24 h after treatment with siRNA; 72 h after spheroid formation (96 h after siRNA treatment), spheroids were embedded in Matrigel. Spheroids were imaged at 0, 24, and 48 h. Data are expressed as increases in spheroid area from 0-h area. Experiments were performed in triplicate, and results are shown as increase in surface area relative to 0-h spheroid area. Data are expressed as average ± SD. *p* values are relative to untreated (untrx) control. $^{**}p < 0.001$. (C) Representative 4× bright-field images. Scale bar, 1000 µm.

with DMSO, IMM-01, or IMM-02 did not induce a subdiploid population (Supplemental Figure S10). Cell counting confirmed that continuous IMM treatment of U251 cells did not dramatically affect cell proliferation through 3 d of treatment, whereas SMIFH2-treated cells showed both reduced cell proliferation after 2 d of treatment and marked inhibition at 3 d of treatment (Supplemental Figure S10). Of interest, IMM compounds also had a minimal effect on nuclear morphologies/phenotypes, with only minor increase in multinuclear cells (Supplemental Figure S10). In contrast, SMIFH2 induced an increase in both fragmented apoptotic nuclei and multinucleation (Supplemental Figure S10). These results are consistent with a recent role proposed for mDia formins in regulating p53 expression, cell proliferation, and nuclear morphologies in response to SMIFH2 treatment (Isogai *et al.*, 2015).

To verify that IMM-01/02-mediated inhibition of spheroid invasion resulted from mDia activation, we introduced recombinant DAD peptide into U87 spheroids via direct protein transfection. DAD expression increases mDia activation, resulting in both increased actin fiber formation and SRF-regulated gene expression (Alberts, 2001). GST-DAD-M1041A served as a control; this mutation prevents binding to and activation of full-length mDia (Alberts, 2001). GST-DAD transfection significantly inhibited spheroid invasion relative to glutathione *S*-transferase (GST) and GST-DAD-M1041A, especially after 24 h (Supplemental Figure S11, A and B). This is not surprising; it is reasonable to expect recombinant proteins to be less stable and therefore less effective at activating endogenous mDia over time.

mDia activation inhibits spheroid invasion in an ex vivo brain-slice invasion model

Although these assays examined 3D invasion, they could not account for stromal and brain microenvironment influences. We therefore examined the effects of SMIFH2, IMM-01, and IMM-02 on spheroid invasion within live cultured rat brain slices. YFP-U87 spheroids were pretreated with DMSO, 40 µM SMIFH2, or 100 µM IMM-01 or IMM-02 for 24 h before placement on 400-µm rat brain slices. Spheroids were maintained in drugs and invaded for 3 or 48 h before confocal imaging. The 3-h time point allowed spheroids to adhere to the brain-slice surface without detectable invasion (Figure 8, A and C).

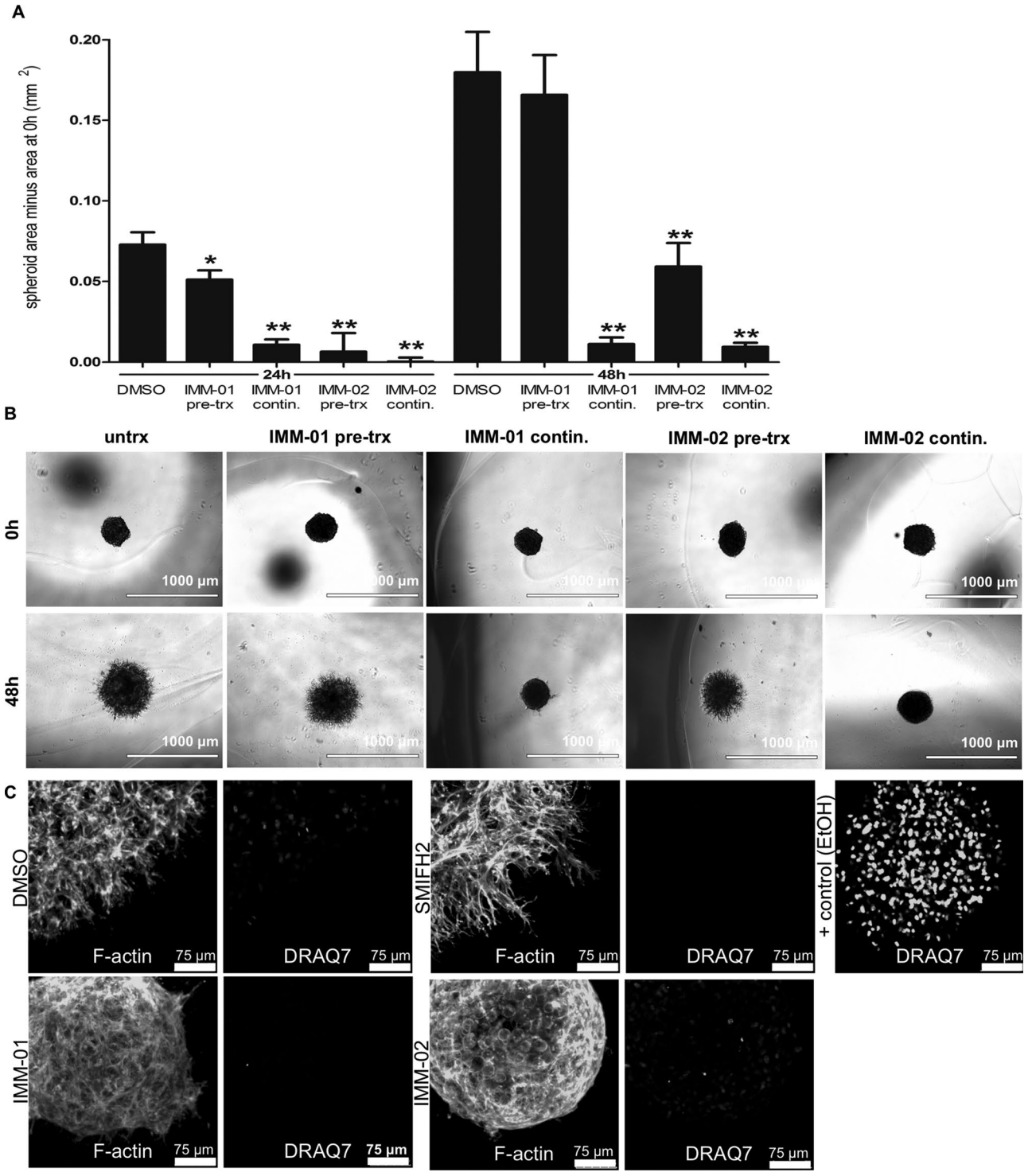

FIGURE 7: Spheroid invasion is inhibited by mDia agonism. (A) U87 spheroids were formed for 72 h, embedded in Matrigel, and treated with DMSO or 100 µM IMM-01 or IMM-02. Spheroids were imaged 0, 24, and 48 h postembedding. Data are expressed as increases in spheroid area from the area at 0 h. Here, "pre-trx" indicates spheroids treated with the indicated compound for 24 h before embedding; "contin." indicates spheroids treated with 100 µM of the indicated compound from 24 h before embedding and throughout the invasion assay. *p* values are relative to DMSO. **p* < 0.05; ***p* < 0.001. All data are expressed as average ± SD. (B) Representative 4× bright-field images after 48-h invasion. Scale bars, 1000 µm. (C) U87 spheroids were formed for 72 h and embedded in GFR Matrigel. Spheroids were invaded for 48 h while being treated with DMSO (control), 40 µM SMIFH2, 100 µM IMM-01, 100 µM IMM-02, or a 50% mixture of ethanol (EtOH):medium (positive control for viability). Spheroids were also treated with DRAQ7 to visualize apoptotic nuclei. Fixed spheroids were stained for F-actin and imaged using confocal microscopy with 2.5-µm *Z*-stacks at 20× images with a 2.25 digital zoom. Representative 3D projections.

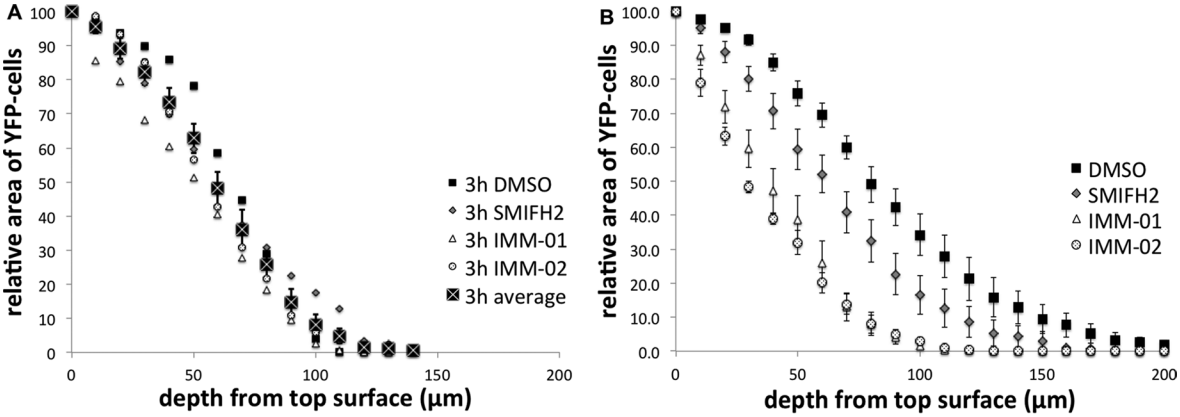

3 hour Depth of Invasion (depth of 50% max surface area)	DMSO	SMIFH2	IMM-01	IMM-02
	67.7	60.7	47.9	56.9
	±7.0	*± 4.9*	*± 20.0*	*± 4.8*
t-test:	*(ns)*	*(ns)*	*(ns)*	*(ns)*

48 hour Depth of Invasion (depth of 50% max surface area)	DMSO	SMIFH2	IMM-01	IMM-02
	85.7	62.2	39.9	31.2
	± 6.2	*± 7.2*	*± 4.1*	*± 1.3*
t-test:		*	*	*

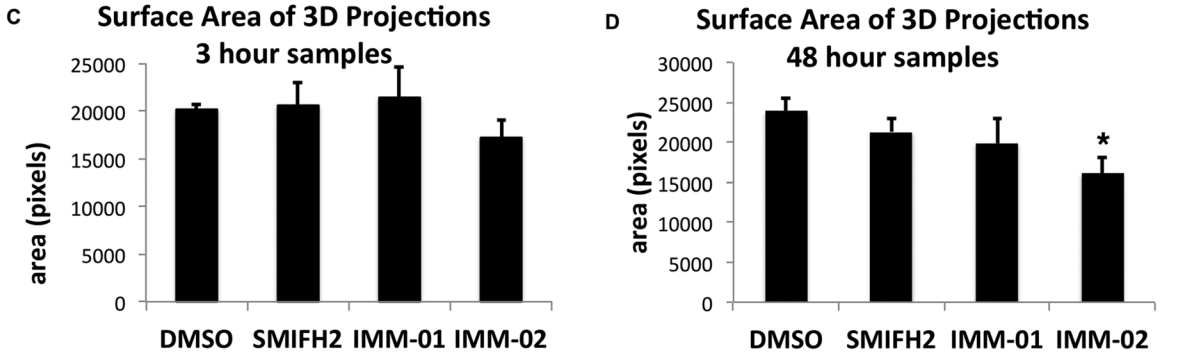

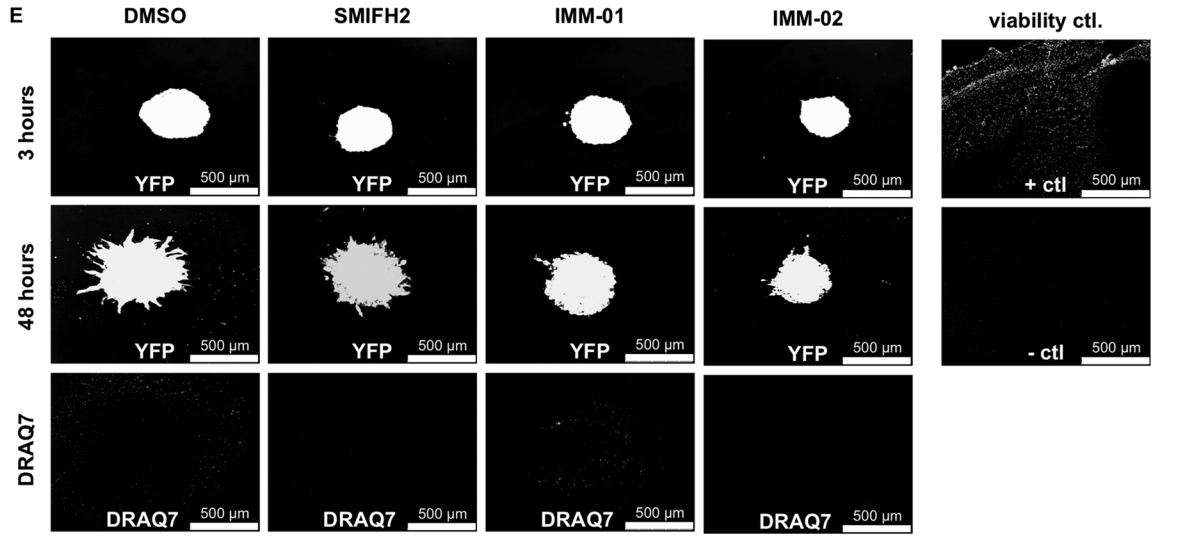

FIGURE 8: Ex vivo rat brain-slice spheroid invasion is inhibited by mDia agonism. (A, B) U87 spheroids were formed for 72 h and pretreated with DMSO, 40 µM SMIFH2, 100 µM IMM-01, or 100 µM IMM-02 for 24 h before being placed on the surfaces of brain slices for invasion assays. Spheroids and brain slices were fixed after 3 (A) or 48 (B) h. Invasion was assessed by confocal microscopy with 10-µm *Z*-stacks and calculating the relative YFP-positive area (which corresponds to glioma cells) for each successive depth. Data are plotted as percentage of maximum surface area corresponding to the surface area of spheroids at the brain-slice surface. Invasion depth was calculated by finding the depth where YFP area equaled 50% of the maximum surface area at the brain-slice surface; *p* values are relative to DMSO. **p* < 0.05. Experiments were performed in duplicate, and data are shown from a representative experiment. (C, D) Three-dimensional projections were created from confocal images, and the YFP-positive projection area for spheroids fixed after 3 (C) or 48 (D) h was calculated to measure cell invasion on the *xy*-axis. *p* values are relative to DMSO. **p* < 0.05. (E) Representative 10× YFP 3D projections after 3 or 48 h of invasion.

Vehicle-treated spheroids substantially invaded within brain slices by 48 h (Figure 8B), and invasive cells were detected >150 µm below the slice surface; SMIFH2 significantly reduced spheroid invasion (Figure 8B). The depth of invasion for SMIFH2-treated spheroids was 62.2 µm. This differed from the result for DMSO-treated spheroids (85.7 µm). In contrast, IMM-01 or IMM-02 treatment more dramatically inhibited invasion, with depths of invasion of 39.9 and 31.2 µm, respectively (Figure 8B).

We then assessed how mDia regulation affects GBM cell invasion away from the spheroid and into the brain slice along the *x*- and *y*-axes by measuring the YFP-positive surface area of 3D projections (Figure 8, C and D). Whereas the YFP-positive surface areas of treated spheroids (3 h) were equivalent (Figure 8C), IMM-02 inhibited invasion in *x*- and *y*-axes relative to DMSO, and SMIFH2 and IMM-01 did not (Figure 8D). Protrusive cells invade away from the DMSO- and SMIFH2-treated spheroid cores, whereas fewer protrusions were seen in IMM-01– and IMM-02–treated spheroids. DRAQ7 was included during the invasion assay for dynamic visualization of nonviable cells. SMIFH2, IMM-01, and IMM-02 treatments resulted in minimal toxicity to brain slices relative to DMSO-treated or ethanol-treated brain slices (Figure 8E). These data indicate that mDia agonism blocks invasion under physiologically relevant conditions and that IMM-01 and IMM-02 do not negatively affect the surrounding brain tissue viability.

DISCUSSION

The inability of current therapeutics to provide more substantial survival benefits for GBM patients is due, in part, to the invasive capacities of tumor cells. Here we delineate the role of mDia formins in GBM cell motility. We reveal a role for mDia in persistent migration (i.e., cell motility in a single direction): loss of mDia function/expression inhibited persistent migration in scratch assays without affecting random migration (i.e., cellular migration with low intrinsic directionality). Conversely, mDia activation through dominant active mDia expression constructs or IMM small-molecule treatment inhibited both intrinsic directional and random migration in scratch assays. In Transwell invasion assays, both mDia inhibition and agonism inhibited chemotactic, single-cell tumor invasion. However, in spheroid invasion assays, mDia inhibition slowed GBM invasion and mDia agonism completely blocked it.

Our findings that mDia inhibition reduced directionally persistent but not random migration points to a role for mDia in the maintenance of glioma cell intrinsic directionality. This is not surprising because Rho small GTP-binding proteins regulate the formation and stabilization of persistent actin-rich protrusions that drive directional migration (Petrie *et al.*, 2009). Decreased Rac1 activity through expression of mutants failing to interact with β1 integrin–promoted directional migration, whereas higher Rac1 activity converted cells into a wandering type of stochastic motility (Pankov *et al.*, 2005). This likely involves downstream effectors, as Rho GTPases work through effectors to stabilize microtubules and polymerize F-actin, thereby promoting cell polarity and directional migration (Fukata *et al.*, 2003). mDia1 was crucial in neutrophil directionally persistent chemotactic migration (Shi *et al.*, 2009). mDia-mediated F-actin assembly supporting the lamella facilitates migration (Gupton *et al.*, 2007); furthermore, mDia can selectively stabilize a subset of microtubules through posttranslational modifications (i.e., acetylation, detyrosination) to promote cell polarity (Fukata *et al.*, 2003) by polarizing the microtubule pool itself (Wen *et al.*, 2004; Gundersen *et al.*, 2005; Eng *et al.*, 2006; Morris *et al.*, 2014).

We found that short-term SMIFH2 treatment inhibited both global β-tubulin expression and microtubule stabilization (Supplemental Figure S5, B and D). The former result is consistent with SMIFH2 treatment in U206 and HCT116 cells (where rapid polymerization/depolymerization cycles were seen, but detyrosination was not assessed; Isogai *et al.*, 2015). Furthermore, SMIFH2 treatment in an *Arabidopsis* model disrupted formin-mediated F-actin dynamics while decreasing microtubule density (Rosero *et al.*, 2013). Collectively these results indicate that the effects of SMIFH2 on microtubule dynamics in response to suppression of formin-mediated F-actin assembly are indeed complex in different models and among formins themselves (Rizvi *et al.*, 2009; Gaillard *et al.*, 2011).

Unexpectedly, IMM treatment failed to stabilize the microtubule array, in contrast to Taxol (Supplemental Figure S5). This was surprising and in contrast with previous results using IMMs in SW480 and NIH3T3 cells, which showed that IMMs led to modest stabilization/detyrosination of microtubules (Lash *et al.*, 2013); the effect was more profound in NIH3T3 fibroblasts maintained before treatment in the absence of serum. Under these conditions, the cells have little or no detyrosinated microtubules, or the stable microtubules "dissolve" or are eliminated. The responses here were similar to what was previously shown in SW480 colon cancer cells; cancer cells may have sufficient "innate" signals that leave a large pool of detyrosinated/stable microtubules present before mDia stimulation with IMMs. Therefore the effects of IMMs on the MT arrays of cancer cells do not appear to be as striking as with the serum-deprived NIH 3T3s stimulated with IMMs.

Future studies should be devoted to establishing a full understanding of the role of formins and their inhibition and activation in the later stages of cell division that precede cytokinesis in tumor cells, where formins have critical roles in abscission (Gopinath *et al.*, 2007; Watanabe *et al.*, 2008). This is important because Taxol kills tumor cells specifically in anaphase by triggering a poorly understood programmed-cell-death response as cells disassemble microtubules to pull apart chromatids. Knowledge of cell death or cytotoxic responses to Taxol and IMMs or formin inhibition in specific tumor cell types needs to be clarified. If IMMs and formin are to be used therapeutically either alone or with Taxol, the mechanism of apoptosis or cell cycle arrest will dictate when they might be most effective as an anticancer strategy. This is important because migration/metastasis and cell division/anaphase are mutually exclusive events.

Alterations in mDia-driven F-actin dynamics via SMIFH2 or IMM treatment, siRNA-mediated depletion, or expression of functional mutants affect U251 GBM cell migration. In the case of formin inhibition through SMIFH2 treatment, this is accompanied by alterations in Golgi polarity in the direction of migration (SMIFH2 treatment, 1 h—the optimal treatment window as previously suggested; Isogai *et al.*, 2015; Figure 3). Juxtanuclear positioning of Golgi is a critical feature of cell migration (Kupfer *et al.*, 1982; Nobes and Hall, 1999). Indeed, F-actin dynamics critically modulates Golgi polarity during cell migration and extension of actin-enriched protrusions (Magdalena *et al.*, 2003; Quassollo *et al.*, 2015). Therefore defects in Golgi polarity may contribute to failure of cells to persistently migrate toward the scratch center (Figure 2 and Supplemental Figure S1). Indeed, a role for mDia formins in establishing Golgi structure and polarity in migratory cancer cells has been postulated (Colon-Franco *et al.*, 2011; Ramabhadran *et al.*, 2011; Zilberman *et al.*, 2011; Isogai *et al.*, 2015). In the case of IMM treatment and formin agonism, Golgi polarization toward the direction of migration was not diminished. Indeed, IMM-02 treatment led to an increase in Golgi polarization toward the wound, albeit not statistically significant relative to controls. It is possible that the increase in F-actin content reduced dynamic Golgi positioning in response to

migratory cues, but further studies are required to fully understand the exact mechanism and kinetics by which IMM treatment affects Golgi positioning in migrating GBM cells.

We propose that mDia agonism and inhibition differentially affect persistent migration by confounding the cellular steering mechanism, or "compass." In cells with balanced mDia activity, directional persistence is maintained through establishment of a single polar leading edge (one compass) with mDia-directed, F-actin–enriched lamellae (Gupton *et al.*, 2007). mDia also directs microtubule tethering, stabilization, and vesicle trafficking at the leading edge to control polarity (Wallar *et al.*, 2007; Zaoui *et al.*, 2008; Daou *et al.*, 2014). mDia agonism would cause migrating cells to lose polarity/persistence by establishing multiple cellular compasses. Sustained mDia agonism disrupts F-actin dynamics and cellular rigidity through enhanced stress fiber production and formation of F-actin–enriched membrane protrusions (Alberts, 2001; Peng *et al.*, 2003; Lash *et al.*, 2013). Thus both persistent and random migration would be affected through loss of net intrinsic asymmetry in the actin- and microtubule-directed migration machinery.

When activated, mDia proteins are believed to interact with barbed ends of F-actin, thereby interfering with dynamic treadmilling associated with filament assembly and vesicle trafficking (Wallar *et al.*, 2007). Disrupting vesicle trafficking to the leading edge could impair persistent migration. In contrast, mDia suppression or functional inhibition drives an apolar cell type lacking a cellular compass or persistent leading edge. Random migration is possible if cells maintain a low intrinsic directionality due to incomplete formin suppression. Random migration also occurs if cells lacking formin activity lose cellular steering mechanisms by negatively affecting recruitment or delivery of signaling proteins driving migration (i.e., Src, Erk) to the leading edge (Tominaga *et al.*, 2000; Gasman *et al.*, 2003; Wallar *et al.*, 2007; Hager *et al.*, 2012). Therefore the impaired persistent migration upon loss of mDia expression/function could result from disrupted cell polarity, altered formation of leading edge structures, or both.

Although Transwell assays simply and effectively screen for invasive behavior, they fail to accurately model in vivo conditions, in which heterogeneous and multicellular cell populations invade in three dimensions (Quail *et al.*, 2012). Because spheroids mimic in vivo growth pattern, histology, and 3D microenvironment, they serve as more accurate models for both invasion and drug screening (Mikhail *et al.*, 2013). Although both SMIFH2 and IMM-01/02 treatments inhibit Transwell invasion, spheroid invasion assays revealed substantial differences between treatments. Transwell invasion was presumably equivalent after mDia inhibition or agonism because the end result (invasion through matrix and accumulation under the membrane) requires directional migration. Therefore, if invasion were assessed through Transwells alone, both strategies would be considered anti-invasive.

IMM-mediated mDia agonism also affects proliferation and induces apoptosis in a colon cancer model (Lash *et al.*, 2013). We failed to detect an increase in apoptosis in two-dimensional U87 monolayers treated with IMM compounds through 120 h, and cell proliferation was only modestly affected through 72 h of treatment, perhaps indicating increased dependence on FH2 domain–containing formins in mediating cell proliferation in SW480 colon cancer and NIH 3T3 cells (Lash *et al.*, 2013). Therefore the effects of IMMs in GBM models may be restricted to anti-invasive activities, a primary therapeutic challenge in GBM treatment. Our current experiments are exploring longer-time GBM spheroid treatment in 3D matrices and in vivo GBM models to definitively test this hypothesis.

In summary, our results offer compelling evidence for mDia agonism through enhanced F-actin dynamics as an effective GBM therapeutic strategy. Our results suggest that mDia inhibition is not an optimal GBM anti-invasive strategy, as it permits cellular motility of low intrinsic directionality through mDia-independent mechanisms. In contrast, mDia agonism blocks motility and is not easily overcome by adaptive mechanisms. Finally, although these results indicate a promising role for mDia formins in blocking GBM spheroid invasion in both in vitro and ex vivo models of invasion, it will be necessary in the immediate future to determine the specific contributions of individual FH2 domain–containing formins (and their isoforms) through knockdown, as the specificity of small-molecule mDia formin agonists and antagonists remains unexplored.

MATERIALS AND METHODS

Cell culture, transfection, plasmids, and time-lapse imaging

U87, U343, U118, T98G, SNF19, SF295, LN229, and A172 glioblastoma cells were a kind gift from William Maltese and Jean Overmeyer (University of Toledo). U251 cells were a kind gift from Marthe Howard (University of Toledo).

Cells were maintained in DMEM (Life Technologies, Grand Island, NY) with 10% FBS (vol/vol), 100 U/ml penicillin, and 100 mg/ml streptomycin in a 37°C incubator with 5% CO_2. For plasmid transfections, U251 cells were transfected with Lipofectamine LTX with Plus reagent (Invitrogen, Grand Island, NY) per the manufacturer's specifications. For siRNA transfection in U251 and U87 cells, Dharmafect ON-TARGETplus SMART-pools (Thermo Scientific, Grand Island, NY) against human DRF1 (mDia1) or DRF3 (mDia2) were used at 50 nM with Dharmafect-1 reagent.

Cell lysates were made using lysis buffer (0.5 M Tris-HCl, pH 6.8, glycerol, 10% [wt/vol] SDS, 0.1% [wt/vol] bromophenol blue) supplemented with dithiothreitol (DTT). Immunoprecipitation lysates were prepared in lysis buffer (20 mM Tris-HCl, pH 7.5, 100 mM NaCl, 1% NP-40, 10% glycerol) containing 0.1 M each sodium vanadate, aprotinin, pepstatin, leupeptin, dithiothreitol, and phenylmethylsulfonyl fluoride (PMSF), and immunoprecipitations were performed as described (Eisenmann *et al.*, 2007a). Rabbit anti-mDia1 (Protein-Tech, Chicago, IL) and mouse anti-mDia2 (AbCam, Cambridge, MA) antibodies were used. Anti–acetylated tubulin antibodies (Glu-tub) were a kind gift from Greg Gundersen (Columbia University). Time-lapse images were acquired with an Olympus IX-81 microscope, Olympus UPlanFL 0.30 NA lens, and environmental chamber that maintained cells at 37°C in a 5% CO_2. Images were acquired at 30-min intervals.

siRNA sequences

siRNAs against human sequences were from Thermoscientific as follows: DIAPH1 pool (LQ-010347); DIAPH3 pool (LQ-018997); individual siRNA for DIAPH3-7 (J-018997-07); and glyceraldehyde-3-phosphate dehydrogenase pool (D-001830).

Immunofluorescence

Cells were fixed with 4% paraformaldehyde (PFA)/phosphate-buffered saline (PBS), permeabilized with 0.2% Triton X-100 (TX100), washed, and incubated with the indicated primary antibody overnight at 4°C. Cells were incubated with Alexa Fluor–labeled secondary antibody (Alexa 488, 546, or 647) and phalloidin (Molecular Probes, Grand Island, NY). Coverslips were mounted onto glass slides with Fluoromount-G (Southern Biotech, Birmingham, AL).

For 3D immunofluorescence, cells were resuspended in GFR-Matrigel (BD Biosciences, San Jose, CA) for 45 min at 37°C before addition of complete medium. Cells were fixed using 4%

PFA, permeabilized using 0.2% TX100, and incubated with primary antibodies overnight at 4°C with fluorescence-labeled secondary antibodies and phalloidin for 3 h at 37°C. A TCS SP5 multiphoton laser-scanning confocal microscope (Leica Microsystems, Buffalo Grove, IL) with a Leica HC PL APO 40X/1.25-0.75 oil CS objective lens generated *Z*-stack images (0.5-µm optical sections), and the Leica AFM acquisition/analytical software suite was used to construct 3D projections.

For 3D spheroid invasion, samples were fixed with 4% paraformaldehyde, permeabilized with 0.2% TX100, and incubated with phalloidin 3h at 37°C. Confocal microscopy was with a Leica 20× HCX PL APO CS Dry UV 0.70NA objective lens to generate Z-stack images (2.5 µm optical sections).

Migration

To calculate the total distance migrated and the directional migration, U251 cells were plated to confluence on a fibronectin-coated glass surface. A scratch was introduced using a sterile pipette tip, and scratch closure was monitored using an inverted IX81 microscope with environmental chamber at 37°C in a 5% CO_2. Acquisition and analysis were performed using MetaMorph software suite. Images of single migrating cells were acquired every 30 min for 24 h. At least 20 cells from at least two independent experiments were tracked individually for each condition. Persistence was calculated as shown in Figure 2, as previously described (Pankov *et al.*, 2005).

Quantifying Golgi polarization

Golgi visualization was performed as described (Etienne-Manneville and Hall, 2001; Fidalgo *et al.*, 2010). Briefly, U251 cells were plated on glass coverslips. Once confluent, coverslips were scratched. Cells were then treated for 1–3 h with DMSO, IMM01, IMM02, or SMIFH2 and allowed to migrate for the duration of the treatment. Cells were fixed and permeabilized as described. Golgi were visualized by staining with anti-gm130 in PBS overnight at 4°C. Cells were then stained for 1.5 h with 1:100 Alexa Fluor–phalloidin 488 in PBS at 37°C, washed thrice, and stained with 20 nM 4′,6-diamidino-2-phenylindole (DAPI) in PBS. Coverslips were then mounted on glass slides using FluoromountG, and cells at the frontmost first cell layer of the wound were visualized on an EVOS fluorescence microscope using an Olympus UPlan Apo 40×/1.00 Oil objective lens. At least 30 cells per treatment from at least two independent experiments were imaged. Quadrants were drawn in Photoshop on each cell such that the frontmost quadrant was facing the direction of the scratch. Positive cells were those whose gm130 staining fell within the frontmost quadrant facing the scratch.

Spheroid formation

U87 spheroids were formed by centrifuging cell suspensions in 0.5% poly-HEMA–coated plates as described (Ivascu and Kubbies, 2006). We resuspended 1000 cells/well in full medium supplemented with 2.5% of 50 µl/ml Matrigel and centrifuged them (1000 × *g*, 10 min). Spheroids were compacted for 72 h at 37°C before use.

U251 spheroids were formed via the hanging-drop method. Cells were resuspended to 10,000 cells/ml, and 50 µl of drops was applied to the lids of 10-cm dishes. Lids were inverted over plates filled with full medium, and spheroids were formed for 72 h at 37°C before use.

Invasion assays

Fluoroblock Transwell inserts with 8-µm pores (BD Biosciences) were coated with fibronectin, after which a gel of 2.5 mg/ml GFR-Matrigel was applied to inserts. We applied 50,000 cells in DMEM containing 0.1% FBS to inserts and placed 10% FBS in the lower chamber. Inserts were stained for 15 min with 0.5 mg/ml calcein AM–fluorescein isothiocyanate (FITC; Invitrogen) in PBS and FITC measured using a fluorescence plate reader at 488 excitation/535 emission. Representative images were acquired using an EVOS-fl digital inverted microscope with an Olympus 10× UPlanFL N 0.30 PhP objective lens. Experiments were performed in triplicate.

For spheroid invasion assays, experiments were performed in triplicate. A thin layer of GFR-Matrigel (6.7 mg/ml) was polymerized in an eight-well chamberglass (Thermoscientific). Spheroids were added, together with an additional layer of Matrigel. Gels were polymerized for 45 min before addition of DMEM containing 20% FBS. Spheroids were imaged using an EVOS-fl digital inverted microscope with an Olympus 4× UPlanFL N 0.13 PhP objective lens at 0–48 h after embedding. MetaMorph software was used to quantify invasion: a region of interest was drawn around each spheroid's invasive front for each time point, and the extent of invasion was calculated as the change in area from 0 h. Representative movies of spheroid invasion were acquired using an IX81 inverted microscope. Images were acquired every 15 min through 48 h with an Olympus 4× UPlanFL 0.13NA objective lens.

Statistical analysis

The total cellular distance migrated and the directional migration components were calculated for at least 20 cells/condition. These values were averaged and expressed as mean ± SD. Spheroid invasion was expressed as the average percentage increase in area relative to 0 h ± SD. Transwell invasion was performed in triplicate and expressed as average relative fluorescence units (RFUs) ± SD. A one-tailed *t* test was performed to evaluate statistical significance with a 95% confidence interval. $p < 0.05$ was considered statistically significant. All error bars are expressed as SD from the experimental mean performed in triplicate, unless otherwise noted. Graphs and statistics were generated in GraphPad Prism software.

Expression and purification of GST-fusion peptides

Rosetta cells (EMD Chemical) expressing pGex-KT fusion constructs were grown overnight in Luria broth (50 µg/ml ampicillin) at 37°C. Expression was induced by adding 0.5 mM isopropyl β-D-1-thiogalactopyranoside with 50 µg/ml ampicillin and incubating overnight at 25°C. The cells were centrifuged at 3000 rpm for 15min at 4°C, resuspended, and sonicated in lysis buffer (TNM buffer: 25 mM Tris, 100 mM NaCl, and 10 mM $MgCl_2$, pH 7.2–7.4) containing 1 mM each PMSF and DTT (Thermoscientific). After centrifugation at 10,000 rpm for 15 min at 4°C, 300 µl of glutathione-agarose (Pharmacia Biotech, Piscataway, NJ) was added to the supernatant and incubated for 5 h at 4°C. After centrifugation at 2000 rpm for 1 min at 4°C, the pellet was washed thrice with TNM buffer containing PMSF and DTT and thrice with TNM buffer without protease inhibitors. The GST-fusion proteins were eluted with 25 mM reduced glutathione (Sigma-Aldrich) TNM buffer for 30 min at 4°C. Glutathione was removed through incubation with 40 µg of GST-agarose (Santa Cruz Biotechnology) for 4 h at 4°C.

Protein transfection

Xfect Protein Transfection Reagent (Clontech, Mountain View, CA) was used per the manufacturer's instructions. For each U87 spheroid, 0.25 µg of recombinant protein was incubated with 5 µl of Xfect protein buffer and 1.5 µl of the Xfect transfection reagent. These were incubated for 30 min, added to the spheroids in 40 µl of serum-free medium, and incubated at 37°C for 24 h.

Microarray data acquisition and analysis

*DIAPH1*and *DIAPH3* expression were assessed in normal human brain and human glioma samples by analyzing publically available Affymetrix whole-genome expression array data from GSE16011 data (Gravendeel *et al.*, 2009; www.ncbi.nlm.nih.gov/geo/query/acc.cgi?acc=GSE16011). *DIAPH1* and *DIAPH3* expression levels were normalized to the respective values of these genes in normal human brain.

Rat brain-slice invasion

All animal experimentation was conducted in accordance with the National Institutes of Health Guide for the Care and Use of Laboratory Animals using protocols approved by the University of Toledo Institutional Animal Use and Care Committee. Ex vivo brain-slice invasion assays were performed as described previously (Jung *et al.*, 2002; Valster *et al.*, 2005). The 400-µm-thick slices were placed in the upper chamber of 0.4-µm–pore size Transwell inserts, which were fed with 2 ml of medium containing 600 U/ml penicillin and 600 µg/ml streptomycin (Life Technologies) plus DMSO or 40 µM SMIFH2 or 100 µM IMM-01 or IMM-02 in the lower chamber and 500 µl in upper chambers. YFP-U87 spheroids were pretreated with DMSO or 40 µM SMIFH2 or 100 µM IMM-01 or IMM-02, placed on the centers of brain slices, and allowed to invade for 3 or 48 h. Drug-containing medium was replaced at 24 h plus 1.5 µM DRAQ7 (Abcam) to assess viability. Brain slices were fixed overnight in 4% paraformaldehyde at 4°C.

To quantify the extent of invasion, Transwell membranes were cut, and brain slices were transferred to glass coverslips before imaging with confocal microscopy. Samples were imaged using a Leica 10× HC PL APO CS Dry UV 0.40NA objective and 3D projections constructed. Slices were imaged for YFP to visualize spheroid invasion into brain slices and DRAQ7 to assess brain slice viability. YFP pixel intensity for 10-µm optical slices was determined, and the extent of invasion into the brain slice was calculated as described (Matsumura *et al.*, 2000), where the area of each successive optical slice was normalized to the maximum area of invasive cells at the brain-slice surface. Invasion depth was calculated as the depth (micrometers) showing half the maximum area of invasive cells.

Cell cycle analysis

Cell cycle analysis using propidium iodide (Sigma-Aldrich) was performed as described (Peng *et al.*, 2007). Whenever possible, a minimum of 10,000 events was collected by flow cytometry (BD FACSCalibur). Data were analyzed using BD CellQuest Pro software, version 6.0.

SRE-LacZ reporter assay

U251 cells were plated on glass-bottom dishes, maintained 14 h in 0.5% fetal calf serum, and then microinjected with an pSRE-lacZ reporter plasmid (0.1 mg/ml) along with 0.1 mg/ml Texas red–coupled dextran (5 kDa) as described previously (Alberts *et al.*, 1998b). After 1 h, cells were treated with 10% (vol/vol) FBS, DMSO, 40 µM SMIFH2, or 100 µM IMM-01 or IMM-02, alone or in combination as indicated. Four hours later, cells were fixed and incubated with X-Gal for 12 h. Blue X-Gal–stained, Texas red–positive cells were counted from three separate experiments in which 20–40 cells were microinjected for each condition.

F-actin quantification by ImageJ

Cellular F-actin was quantified in U251 plated on glass coverslips by measuring fluorescence from phalloidin–Alexa Fluor 546 as described previously (Burgess *et al.*, 2010; Gavet and Pines, 2010; Potapova *et al.*, 2011; McCloy *et al.*, 2014). Briefly, cells were treated for 1–3 h with the indicated treatments and fixed and permeabilized as described. Cells were stained with 1:200 phalloidin–Alexa Fluor 546 for 45 min at 37°C. Coverslips were washed thrice and stained with 20 nM DAPI in PBS. Coverslips were then mounted on glass slides using FluoromountG, and cells were visualized on an EVOS fluorescence microscope using an Olympus UPlan Apo 40×/1.00 Oil objective lens. Cells were then traced using ImageJ, and corrected total cell fluorescence values were calculated as described (Burgess *et al.*, 2010; Gavet and Pines, 2010; Potapova *et al.*, 2011; McCloy *et al.*, 2014). At least 30 cells per coverslip were counted, and the experiment was repeated at least twice.

ACKNOWLEDGMENTS

We thank members of the Eisenmann lab, Betty Groff, Lot R. Haak, and David Nadziejka for critical reading of the manuscript and helpful discussion; Stephanie Weber, Jessica Saul, and Jacob Justinger for technical assistance; and the University of Toledo Advanced Microscopy and Imaging Core for imaging assistance. This work was supported by the University of Toledo Foundation (K.M.E.), the National Cancer Institute (R01CA151632; K.M.E.), a University of Toledo Translational Research Stimulation Award (K.M.E.), and the Van Andel Foundation (A.S.A.).

REFERENCES

Alberts AS (2001). Identification of a carboxyl-terminal diaphanous-related formin homology protein autoregulatory domain. J Biol Chem 276, 2824–2830.

Alberts AS, Bouquin N, Johnston LH, Treisman R (1998a). Analysis of RhoA-binding proteins reveals an interaction domain conserved in heterotrimeric G protein beta subunits and the yeast response regulator protein Skn7. J Biol Chem 273, 8616–8622.

Alberts AS, Geneste O, Treisman R (1998b). Activation of SRF-regulated chromosomal templates by Rho-family GTPases requires a signal that also induces H4 hyperacetylation. Cell 92, 475–487.

Ang SF, Zhao ZS, Lim L, Manser E (2010). DAAM1 is a formin required for centrosome re-orientation during cell migration. PLoS One 5, e13064.

Baarlink C, Brandt D, Grosse R (2010). SnapShot: formins. Cell 142, 172, 172 e171.

Batchelor T, Gerstner ER, Emblem KE, Duda DG, Katpathy-Cramer J, Snuderl M, Ancukiewicz M, Polaskova P, Pinho MC, Jennings D, *et al.* (2013). Improved tumor oxygenation and survival in glioblastoma patients who show increased blood perfusion after cediranib and chemoradiation. Proc Natl Acad Sci USA 110, 19059–19064.

Berens ME, Giese A (1999). "…those left behind." Biology and oncology of invasive glioma cells. Neoplasia 1, 208–219.

Burgess A, Vigneron S, Brioudes E, Labbe JC, Lorca T, Castro A (2010). Loss of human Greatwall results in G2 arrest and multiple mitotic defects due to deregulation of the cyclin B-Cdc2/PP2A balance. Proc Natl Acad Sci USA 107, 12564–12569.

Chesarone MA, DuPage AG, Goode BL (2010). Unleashing formins to remodel the actin and microtubule cytoskeletons. Nat Rev Mol Cell Biol 11, 62–74.

Colon-Franco JM, Gomez TS, Billadeau DD (2011). Dynamic remodeling of the actin cytoskeleton by FMNL1gamma is required for structural maintenance of the Golgi complex. J Cell Sci 124, 3118–3126.

Copeland JW, Treisman R (2002). The diaphanous-related formin mDia1 controls serum response factor activity through its effects on actin polymerization. Mol Biol Cell 13, 4088–4099.

Daou P, Hasan S, Breitsprecher D, Baudelet E, Camoin L, Audebert S, Goode BL, Badache A (2014). Essential and nonredundant roles for Diaphanous formins in cortical microtubule capture and directed cell migration. Mol Biol Cell 25, 658–668.

Del Duca D, Werbowetski T, Del Maestro RF (2004). Spheroid preparation from hanging drops: characterization of a model of brain tumor invasion. J Neurooncol 67, 295–303.

DeWard AD, Eisenmann KM, Matheson SF, Alberts AS (2010). The role of formins in human disease. Biochim Biophys Acta 1803, 226–233.

Dolecek TA, Propp JM, Stroup NE, Kruchko C (2012). CBTRUS statistical report: primary brain and central nervous system tumors diagnosed in the United States in 2005–2009. Neuro-oncology 14(Suppl 5), 1–49.
Eisenmann KM, Harris ES, Kitchen SM, Holman HA, Higgs HN, Alberts AS (2007a). Dia-interacting protein modulates formin-mediated actin assembly at the cell cortex. Curr Biol 17, 579–591.
Eisenmann KM, West RA, Hildebrand D, Kitchen SM, Peng J, Sigler R, Zhang J, Siminovitch KA, Alberts AS (2007b). T cell responses in mammalian diaphanous-related formin mDia1 knock-out mice. J Biol Chem 282, 25152–25158.
Eng CH, Huckaba TM, Gundersen GG (2006). The formin mDia regulates GSK3beta through novel PKCs to promote microtubule stabilization but not MTOC reorientation in migrating fibroblasts. Mol Biol Cell 17, 5004–5016.
Etienne-Manneville S, Hall A (2001). Integrin-mediated activation of Cdc42 controls cell polarity in migrating astrocytes through PKCzeta. Cell 106, 489–498.
Fidalgo M, Fraile M, Pires A, Force T, Pombo C, Zalvide J (2010). CCM3/PDCD10 stabilizes GCKIII proteins to promote Golgi assembly and cell orientation. J Cell Sci 123, 1274–1284.
Fukata M, Nakagawa M, Kaibuchi K (2003). Roles of Rho-family GTPases in cell polarisation and directional migration. Curr Opin Cell Biol 15, 590–597.
Gaillard J, Ramabhadran V, Neumanne E, Gurel P, Blanchoin L, Vantard M, Higgs HN (2011). Differential interactions of the formins INF2, mDia1, and mDia2 with microtubules. Mol Biol Cell 22, 4575–4587.
Gasman S, Kalaidzidis Y, Zerial M (2003). RhoD regulates endosome dynamics through Diaphanous-related Formin and Src tyrosine kinase. Nat Cell Biol 5, 195–204.
Gauvin TJ, Fukui J, Peterson JR, Higgs HN (2009). Isoform-selective chemical inhibition of mDia-mediated actin assembly. Biochemistry 48, 9327–9329.
Gavet O, Pines J (2010). Progressive activation of CyclinB1-Cdk1 coordinates entry to mitosis. Dev Cell 18, 533–543.
Geneste O, Copeland JW, Treisman R (2002). LIM kinase and Diaphanous cooperate to regulate serum response factor and actin dynamics. J Cell Biol 157, 831–838.
Giese A, Bjerkvig R, Berens ME, Westphal M (2003). Cost of migration: invasion of malignant gliomas and implications for treatment. J Clin Oncol 21, 1624–1636.
Giese A, Loo MA, Tran N, Haskett D, Coons SW, Berens ME (1996). Dichotomy of astrocytoma migration and proliferation. Int J Cancer J 67, 275–282.
Gopinath SD, Narumiya S, Dhawan J (2007). The RhoA effector mDiaphanous regulates MyoD expression and cell cycle progression via SRF-dependent and SRF-independent pathways. J Cell Sci 120, 3086–3098.
Gorelik R, Yang C, Kameswaran V, Dominguez R, Svitkina T (2011). Mechanisms of plasma membrane targeting of formin mDia2 through its amino terminal domains. Mol Biol Cell 22, 189–201.
Gravendeel LA, Kouwenhoven MC, Gevaert O, de Rooi JJ, Stubbs AP, Duijm JE, Daemen A, Bleeker FE, Bralten LB, Kloosterhof NK, *et al.* (2009). Intrinsic gene expression profiles of gliomas are a better predictor of survival than histology. Cancer Res 69, 9065–9072.
Grosse R, Copeland JW, Newsome TP, Way M, Treisman R (2003). A role for VASP in RhoA-Diaphanous signalling to actin dynamics and SRF activity. EMBO J 22, 3050–3061.
Grossman SA, Ye X, Piantadosi S, Desideri S, Nabors LB, Rosenfeld M, Fisher J, Consortium NC (2010). Survival of patients with newly diagnosed glioblastoma treated with radiation and temozolomide in research studies in the United States. Clin Cancer Res 16, 2443–2449.
Gundersen GG, Wen Y, Eng CH, Schmoranzer J, Cabrera-Poch N, Morris EJ, Chen M, Gomes ER (2005). Regulation of microtubules by Rho GTPases in migrating cells. Novartis Found Symp 269, 106–116; discussion, 116–126, 223–230.
Gupton SL, Eisenmann K, Alberts AS, Waterman-Storer CM (2007). mDia2 regulates actin and focal adhesion dynamics and organization in the lamella for efficient epithelial cell migration. J Cell Sci 120, 3475–3487.
Hager MH, Morley S, Bielenberg DR, Gao S, Morello M, Holcomb IN, Liu W, Mouneimne G, Demichelis F, Kim J, *et al.* (2012). DIAPH3 governs the cellular transition to the amoeboid tumour phenotype. EMBO Mol Med 4, 743–760.
Harris ES, Rouiller I, Hanein D, Higgs HN (2006). Mechanistic differences in actin bundling activity of two mammalian formins, FRL1 and mDia2. J Biol Chem 281, 14383–14392.
Hsieh CH, Chang HT, Shen WC, Shyu WC, Liu RS (2012). Imaging the impact of Nox4 in cycling hypoxia-mediated U87 glioblastoma invasion and infiltration. Mol Imaging Biol 14, 489–499.
Isogai T, van der Kammen R, Innocenti M (2015). SMIFH2 has effects on Formins and p53 that perturb the cell cytoskeleton. Sci Rep 5, 9802.
Ivascu A, Kubbies M (2006). Rapid generation of single-tumor spheroids for high-throughput cell function and toxicity analysis. J Biomol Screening 11, 922–932.
Jung S, Kim HW, Lee JH, Kang SS, Rhu HH, Jeong YI, Yang SY, Chung HY, Bae CS, Choi C, *et al.* (2002). Brain tumor invasion model system using organotypic brain-slice culture as an alternative to in vivo model. J Cancer Res Clin Oncol 128, 469–476.
Kovar DR (2006). Molecular details of formin-mediated actin assembly. Curr Opin Cell Biol 18, 11–17.
Kupfer A, Louvard D, Singer SJ (1982). Polarization of the Golgi apparatus and the microtubule-organizing center in cultured fibroblasts at the edge of an experimental wound. Proc Natl Acad Sci USA 79, 2603–2607.
Lammers M, Rose R, Scrima A, Wittinghofer A (2005). The regulation of mDia1 by autoinhibition and its release by Rho*GTP. EMBO J 24, 4176–4187.
Lash LL, Wallar BJ, Turner JD, Vroegop SM, Kilkuskie RE, Kitchen-Goosen SM, Xu HE, Alberts AS (2013). Small-molecule intramimics of formin autoinhibition: a new strategy to target the cytoskeletal remodeling machinery in cancer cells. Cancer Res 73, 6793–6803.
Lefranc F, Brotchi J, Kiss R (2005). Possible future issues in the treatment of glioblastomas: special emphasis on cell migration and the resistance of migrating glioblastoma cells to apoptosis. J Clin Oncol 23, 2411–2422.
Magdalena J, Millard TH, Machesky LM (2003). Microtubule involvement in NIH 3T3 Golgi and MTOC polarity establishment. J Cell Sci 116, 743–756.
Mariani L, Beaudry C, McDonough WS, Hoelzinger DB, Demuth T, Ross KR, Berens T, Coons SW, Watts G, Trent JM, *et al.* (2001). Glioma cell motility is associated with reduced transcription of proapoptotic. J Neuro-Oncol 53, 161–176.
Matsumura H, Ohnishi T, Kanemura Y, Maruno M, Yoshimine T (2000). Quantitative analysis of glioma cell invasion by confocal laser scanning microscopy in a novel brain slice model. Biochem Biophys Res Commun 269, 513–520.
McCloy RA, Rogers S, Caldon CE, Lorca T, Castro A, Burgess A (2014). Partial inhibition of Cdk1 in G 2 phase overrides the SAC and decouples mitotic events. Cell Cycle 13, 1400–1412.
Mikhail AS, Eetezadi S, Allen C (2013). Multicellular tumor spheroids for evaluation of cytotoxicity and tumor growth inhibitory effects of nanomedicines in vitro: a comparison of docetaxel-loaded block copolymer micelles and Taxotere(R). PLoS One 8, e62630.
Milano MT, Okunieff P, Donatello RS, Mohile NA, Sul J, Walter KA, Korones DN (2010). Patterns and timing of recurrence after temozolomide-based chemoradiation for glioblastoma. Int J Radiat Oncol Biol Phys 78, 1147–1155.
Morris EJ, Nader GP, Ramalingam N, Bartolini F, Gundersen GG (2014). Kif4 interacts with EB1 and stabilizes microtubules downstream of Rho-mDia in migrating fibroblasts. PLoS One 9, e91568.
Nakada M, Nakada S, Demuth T, Tran NL, Hoelzinger DB, Berens ME (2007). Molecular targets of glioma invasion. Cell Mol Life Sci 64, 458–478.
Nezami AG, Poy F, Eck MJ (2006). Structure of the autoinhibitory switch in formin mDia1. Structure 14, 257–263.
Nobes CD, Hall A (1999). Rho GTPases control polarity, protrusion, and adhesion during cell movement. J Cell Biol 144, 1235–1244.
Palazzo AF, Cook TA, Alberts AS, Gundersen GG (2001). mDia mediates Rho-regulated formation and orientation of stable microtubules. Nat Cell Biol 3, 723–729.
Pankov R, Endo Y, Even-Ram S, Araki M, Clark K, Cukierman E, Matsumoto K, Yamada KM (2005). A Rac switch regulates random versus directionally persistent cell migration. J Cell Biol 170, 793–802.
Peng J, Kitchen SM, West RA, Sigler R, Eisenmann KM, Alberts AS (2007). Myeloproliferative defects following targeting of the Drf1 gene encoding the mammalian diaphanous related formin mDia1. Cancer Res 67, 7565–7571.
Peng J, Wallar BJ, Flanders A, Swiatek PJ, Alberts AS (2003). Disruption of the Diaphanous-related formin Drf1 gene encoding mDia1 reveals a role for Drf3 as an effector for Cdc42. Curr Biol 13, 534–545.
Petrie RJ, Doyle AD, Yamada KM (2009). Random versus directionally persistent cell migration. Nat Rev Mol Cell Biol 10, 538–549.

Pettee KM, Dvorak KM, Nestor-Kalinoski AL, Eisenmann KM (2014). An mDia2/ROCK signaling axis regulates invasive egress from epithelial ovarian cancer spheroids. PLoS One 9, e90371.
Potapova TA, Sivakumar S, Flynn JN, Li R, Gorbsky GJ (2011). Mitotic progression becomes irreversible in prometaphase and collapses when Wee1 and Cdc25 are inhibited. Mol Biol Cell 22, 1191–1206.
Quail DF, Maciel TJ, Rogers K, Postovit LM (2012). A unique 3D in vitro cellular invasion assay. J Biomol Screen 17, 1088–1095.
Quassollo G, Wojnacki J, Salas DA, Gastaldi L, Marzolo MP, Conde C, Bisbal M, Couve A, Caceres A (2015). A RhoA signaling pathway regulates dendritic Golgi outpost formation. Curr Biol 25, 971–982.
Radaelli E, Ceruti R, Patton V, Russo M, Degrassi A, Croci V, Caprera F, Stortini G, Scanziani E, Pesenti E, Alzani R (2009). Immunohistopathological and neuroimaging characterization of murine orthotopic xenograft models of glioblastoma multiforme recapitulating the most salient features of human disease. Histol Histopathol 24, 879–891.
Ramabhadran V, Korobova F, Rahme GJ, Higgs HN (2011). Splice variant-specific cellular function of the formin INF2 in maintenance of Golgi architecture. Mol Biol Cell 22, 4822–4833.
Rizvi SA, Neidt EM, Cui J, Feiger Z, Skau CT, Gardel ML, Kozmin SA, Kovar DR (2009). Identification and characterization of a small molecule inhibitor of formin-mediated actin assembly. Chem Biol 16, 1158–1168.
Rosero A, Zarsky V, Cvrckova F (2013). AtFH1 formin mutation affects actin filament and microtubule dynamics in Arabidopsis thaliana. J Exp Bot 64, 585–597.
Shi Y, Zhang J, Mullin M, Dong B, Alberts AS, Siminovitch KA (2009). The mDial formin is required for neutrophil polarization, migration, and activation of the LARG/RhoA/ROCK signaling axis during chemotaxis. J Immunol 182, 3837–3845.
Sotiropoulos A, Gineitis D, Copeland J, Treisman R (1999). Signal-regulated activation of serum response factor is mediated by changes in actin dynamics. Cell 98, 159–169.
Strojnik T, Kavalar R, Lah TT (2006). Experimental model and immunohistochemical analyses of U87 human glioblastoma cell xenografts in immunosuppressed rat brains. Anticancer Res 26, 2887–2900.
Tominaga T, Sahai E, Chardin P, McCormick F, Courtneidge SA, Alberts AS (2000). Diaphanous-related formins bridge Rho GTPase and Src tyrosine kinase signaling. Mol Cell 5, 13–25.
Valster A, Tran NL, Nakada M, Berens ME, Chan AY, Symons M (2005). Cell migration and invasion assays. Methods 37, 208–215.
Wallar BJ, Alberts AS (2003). The formins: active scaffolds that remodel the cytoskeleton. Trends Cell Biol 13, 435–446.
Wallar BJ, Deward AD, Resau JH, Alberts AS (2007). RhoB and the mammalian Diaphanous-related formin mDia2 in endosome trafficking. Exp Cell Res 313, 560–571.
Watanabe S, Ando Y, Yasuda S, Hosoya H, Watanabe N, Ishizaki T, Narumiya S (2008). mDia2 induces the actin scaffold for the contractile ring and stabilizes its position during cytokinesis in NIH 3T3 cells. Mol Biol Cell 19, 2328–2338.
Watanabe N, Madaule P, Reid T, Ishizaki T, Watanabe G, Kakizuka A, Saito Y, Nakao K, Jockusch BM, Narumiya S (1997). p140mDia, a mammalian homolog of Drosophila diaphanous, is a target protein for Rho small GTPase and is a ligand for profilin. EMBO J 16, 3044–3056.
Wen Y, Eng CH, Schmoranzer J, Cabrera-Poch N, Morris EJ, Chen M, Wallar BJ, Alberts AS, Gundersen GG (2004). EB1 and APC bind to mDia to stabilize microtubules downstream of Rho and promote cell migration. Nat Cell Biol 6, 820–830.
Zaoui K, Honore S, Isnardon D, Braguer D, Badache A (2008). Memo-RhoA-mDia1 signaling controls microtubules, the actin network, and adhesion site formation in migrating cells. J Cell Biol 183, 401–408.
Zilberman Y, Alieva NO, Miserey-Lenkei S, Lichtenstein A, Kam Z, Sabanay H, Bershadsky A (2011). Involvement of the Rho-mDia1 pathway in the regulation of Golgi complex architecture and dynamics. Mol Biol Cell 22, 2900–2911.